

PAPER DETAILS

TITLE: Removal of Naphthol Blue Black by Heterogeneous Fenton-like Reaction with (Bimetallic Iron-Zinc Nanoparticles)/Carbon Composite Material

AUTHORS: Deniz UZUNOGLU,Ege KARADENİZ,Ayla ÖZER

PAGES: 41-54

ORIGINAL PDF URL: <https://dergipark.org.tr/tr/download/article-file/866263>



Removal of Naphthol Blue Black by Heterogeneous Fenton-like Reaction with (Bimetallic Iron-Zinc Nanoparticles)/Carbon Composite Material

Deniz UZUNOĞLU* , Ege KARADENİZ , Ayla ÖZER 

Mersin University, Department of Chemical Engineering, Mersin, Turkey.

Abstract: In this work, the synthesis and characterization of (Fe-Zn NPs)/C were carried out and then it was evaluated as a heterogeneous catalyst in the Fenton-like reaction of Naphthol Blue Black (NBB). The characterization studies showed that the synthesized composite material had an amorphous structure and it contained the elements C, O, Fe, and Zn. In addition, it was observed by SEM analysis that iron-zinc nanoparticles (Fe-Zn NPs) were formed between the carbon microspheres indicating the hydrochar structure. The Fenton-like removal ability of (Fe-Zn NPs)/C was also evaluated and the results demonstrated that (Fe-Zn NPs)/C could be a promising Fenton-like catalyst for the removal of NBB from aqueous solutions. The optimum experimental conditions of this Fenton-like reaction were determined to be as follows: Initial pH was 3.0, H₂O₂ concentration was 50 mM, temperature was 40 °C, and catalyst concentration was 0.25 g/L. The reaction order and rate constant were found as 0.5669 and 4.45, respectively.

Keywords: Composite material, Fenton-like reaction, Heterogeneous catalyst, Hydrochar, Naphthol Blue Black, Wastewater treatment.

Submitted: November 29, 2019. **Accepted:** November 01, 2020.

Cite this: Uzunoğlu D, Karadeniz E, Özer A. Removal of Naphthol Blue Black by Heterogeneous Fenton-like Reaction with (Bimetallic Iron-Zinc Nanoparticles)/Carbon Composite Material. JOTCSB. 41-54;3(2):41-54.

***Corresponding author. E-mail:** denizuzunoglu4@gmail.com.

INTRODUCTION

The rapid urbanization and industrialization have recently caused a serious environmental concern due to the huge amount of wastewater generation. The paper, textiles, dyeing of cloth, printing, pharmaceutical, and cooking industries generate the large quantities of colored wastewater due to the use of dyestuffs (1). The unrestrained discharge of these colored wastewaters into the receiving waters negatively affects the aquatic life and also human life via nutrient cycle because the dyestuffs are mostly toxic, carcinogenic, mutagenic or allergenic (2). Therefore, these types of wastewaters must be treated according to the regulations prior to the discharge of them. There are many physical (coagulation, flocculation, adsorption, ion exchange, membrane filtration, nano filtration, ultra-filtration, reverse osmosis), chemical (advanced oxidation process, electrochemical destruction, ozonation, ultraviolet irradiation), and biological (degradation with algae/enzyme/bacteria, combination of aerobic-anaerobic conditions, adsorption by microbial

biomass) methods for the removal of dyestuffs from wastewaters (3). Among them, the advanced oxidation processes (AOP) based on the production of free radicals, such as Fenton, photo-Fenton, sono-Fenton processes, ozonation, electrochemical oxidation, photolysis with H₂O₂, and O₃ electro-Fenton, have great importance for the treatment of the wastewaters containing the dyestuffs, which are difficult to remove by conventional methods. In the Fenton processes, highly oxidizing •OH radicals are used to oxidize the dyestuffs. It provides the degradation of complex structured dyestuffs to smaller organic molecules or the completely oxidation of it to CO₂ and H₂O (4). Homogeneous Fenton process, in which soluble iron acts as the catalyst, has been extensively studied and widely applied commercially for the dyestuff treatment (5). However, the difficulty of the homogenous catalyst recovery and tight pH range for reaction are reported as disadvantages (6). In order to overcome these disadvantages of the homogeneous Fenton process, some attempts have been made to develop heterogeneous catalysts, especially iron based

nanoparticles. The metallic and bimetallic iron nanoparticles can be synthesized by various methods such as chemical precipitation, microemulsion, hydrothermal synthesis, thermal degradation, sonochemical synthesis, and electrochemical deposition (7). The most common disadvantages of the metallic nanoparticles is the leaching of metal ions to the medium and the aggregation of them, resulting in a low catalytic activity (8,9). In order to improve the catalyst activity (to prevent the leaching and the aggregation) of the nanoparticles synthesized by these methods, the nanoparticles can be combined with various carbonaceous materials such as cellulose, glucose, agricultural waste, animal manure, food waste, and so on (10). Hydrochar, which is a solid product from a carbonization process of these biomasses, has attracted much attention due to its unique properties. Several thermochemical methods such as combustion, aerial gasification, pyrolysis, and hydrothermal carbonization could be applied for the carbonization process. Among them, the hydrothermal carbonization method have the advantages of being more economical and easy applicability. The hydrothermal carbonization could be carried out at mild conditions (180-250 °C and 20-40 bar) and it does not require pre-drying unlike other methods (11). In the literature, hydrochar has been widely used for supporting various nanoparticles and these hydrochar supported-nanoparticles could be effectively used in the catalytic wastewater treatment processes. For instance, Liang et al. (2017) have investigated the heterogeneous photo-Fenton degradation of organic pollutants with amorphous Fe-Zn-oxide/hydrochar under visible light irradiation (12); Ma et al. (2018) have evaluated the iron nanoparticles in situ encapsulated in lignin-derived hydrochar as an effective catalyst for phenol removal(8); Khataee et al. (2017) have studied on the ultrasound-assisted removal of Acid Red 17 using nanosized Fe₃O₄-loaded coffee waste hydrochar (15); Liu et al. (2016) have reported that nanoscale zerovalent iron loaded on porous carbon showed high performance for removal of carcinogenic polychlorinated biphenyls from aqueous solutions (16); Gai et al. (2017) used the iron nanoparticles immobilized into the porous hydrochar for catalytic decomposition of phenol (17). In this respect, (bimetallic iron-zinc nanoparticles)/carbon composite material [(Fe-Zn NPs)/C] was synthesized by combined coprecipitation/hydrothermal carbonization method and then, [(Fe-ZnNPs)/C] was evaluated as a heterogeneous catalyst in the Fenton-like reaction of Naphthol Blue Black (NBB) dyestuff.

EXPERIMENTAL SECTION

Materials

Fe(NO₃)₃·9H₂O (Acros), ZnCl₂ (Merck), D-glucose (Alfa-Aesar), NaOH (Merck), HCl (Sigma-Aldrich),

H₂O₂ (Merck), NBB (Merck) are of analytical grade and they were used without any purification.

Synthesis and Characterization of (Bimetallic Iron-Zinc Nanoparticles)/Carbon Composite Material

In the synthesis of (bimetallic iron-zinc nanoparticles)/carbon composite material [(Fe-Zn NPs)/C]; Fe(NO₃)₃, Zn(NO₃)₂, and D-glucose were dissolved in 60 mL of distilled water and then, the solution pH was adjusted to 11 with the NaOH solution and it was magnetically stirred for 1.0 h. After that, the obtained black-colored suspension containing bimetallic Fe-Zn NPs was autoclaved at 130 °C for 10 h in a Teflon-lined stainless steel autoclave. After the autoclave process, [(Fe-ZnNPs)/C] was obtained and then, it was washed several times with distilled water and dried at 110 °C for 6 h. [(Fe-ZnNPs)/C] was stored in the refrigerator at +4 °C for further experiments (12). The characterization of [(Fe-ZnNPs)/C] was performed using Scanning Electron Microscope (SEM-Zeiss/Supra 55, Germany), Energy Dispersive X-ray Spectroscopy (EDX- Zeiss/Supra 55, Germany), and Powder X-ray Diffractometer (XRD-Philips XPert, Netherlands).

Removal of Naphthol Blue Black via Fenton-like Reaction

In the Fenton-like experiments, the desired amount of (Fe-Zn NPs)/C was added to 100 mL of NBB dyestuff solutions at desired initial pH and initial dye concentrations. The flasks containing the solutions were agitated in the water bath for 30 minutes to make certain desorption-adsorption equilibrium of NBB dyestuff aqueous solution with the catalyst. Then, 5 mL of H₂O₂ solution were added to the aqueous dyestuff solutions including the catalyst. After that, the samples were taken at pre-determined time intervals and the catalyst were removed by centrifugation. The concentration of NBB dyestuff was observed by using the UV-Vis spectrophotometer at 628 nm wavelength. The decolorization percentage for NBB dyestuff was expressed in terms of the decrease in UV-Vis absorbance. All of experiments were performed in triplicate and the results were presented as the mean of these experiments.

RESULTS AND DISCUSSIONS

Characterization of (Fe-Zn NPs)/C

The structure and phase purity of (Fe-Zn NPs)/C were investigated by XRD analysis. The obtained XRD pattern of (Fe-Zn NPs)/C was given in Figure 1. Accordingly, narrow and sharp peaks showing a certain crystal structure could not be obtained; however, only a wide peak was obtained at 20°, which is related to the amorphous and non-graphite carbon structure (12-14). As a result, the composite material synthesized in this study does not have a specific crystalline structure; it is an amorphous

material.

The elemental content of (Fe-Zn NPs)/C was determined by EDX analysis. The corresponding SEM image of (Fe-Zn NPs)/C and EDX mapping images were shown in Figures 2 (a)-(f). Accordingly, the microspheres had the element of carbon

indicating the structure of a hydrochar while the iron-zinc nanoparticles (Fe-Zn NPs) formed between the microspheres had the elements of iron, zinc, and oxygen. Besides, (Fe-Zn NPs)/C contained 58 %, 12 %, 19 %, and 10% by mass of carbon, oxygen, iron, and zinc elements, respectively.

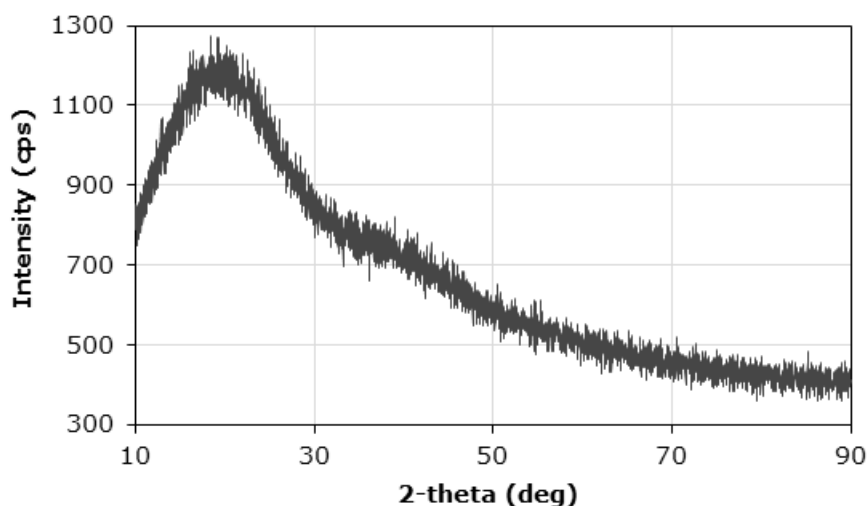


Figure 1. XRD pattern of (Fe-Zn NPs)/C.

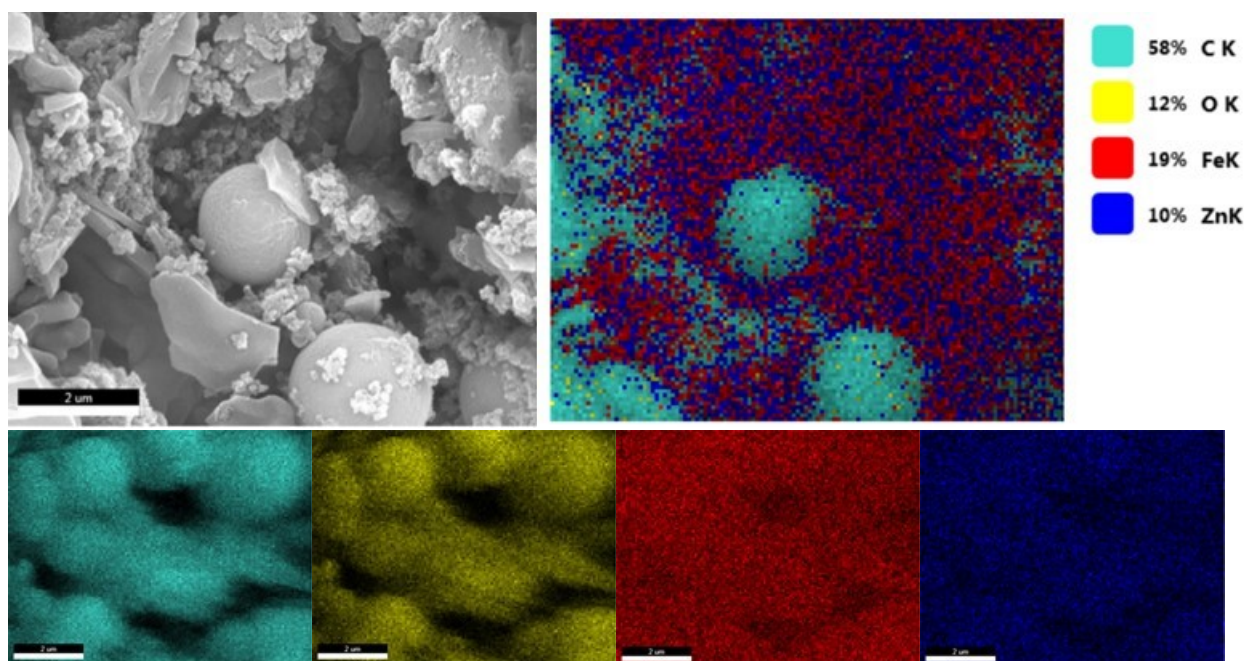


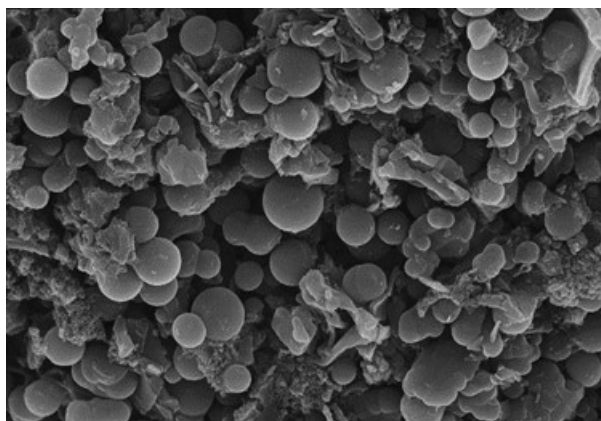
Figure 2. (a) The corresponding SEM image of (Fe-Zn NPs)/C, (b) EDX mapping image of (Fe-Zn NPs)/C, (c) Carbon mapping, (d) Oxygen mapping, (e) Iron mapping, (f) Zinc mapping.

In this study, (Fe-Zn NPs)/C as well as [(Fe NPs)/C] and [(Zn NPs)/C] were synthesized and their morphologies were investigated by SEM analysis given in Figure 3 (a)-(j). According to Figure 3(a) and (b), it was observed that the (Fe-Zn NPs) formed between the carbon microspheres indicating the hydrochar structure as observed in EDX analysis. The blown-up images of the nanoparticles between the microspheres was presented in Figure

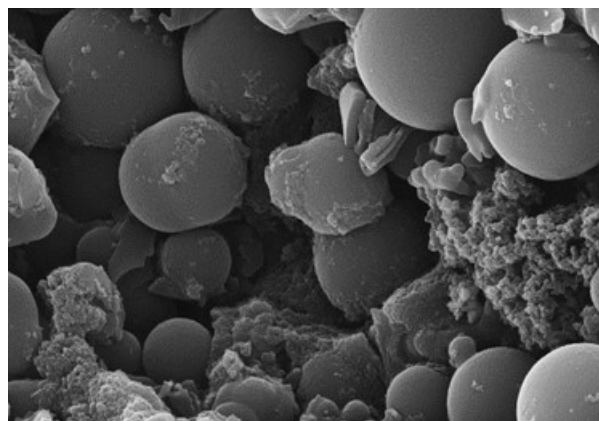
3(c) and (d). SEM images of (Fe-Zn NPs)/C after the Fenton-like reaction were given in Figures 3(e) and (f). The mean particle size of the nanoparticles before the Fenton-like reaction was calculated as 37.43 ± 2.77 nm by Image-J program whilst this value was calculated as 68.84 ± 8.79 nm after the removal of NBB dyestuff via Fenton-like reaction. This particle size analysis via Image-J program was performed with at least 100 particles. As a result,

mostly regular spherical nanoparticles were observed before the Fenton-like reaction while after the Fenton-like reaction, both the particle size increased due to the agglomeration of the nanoparticles, and the regular spherical forms of the nanoparticles destroyed. It could be clearly seen in

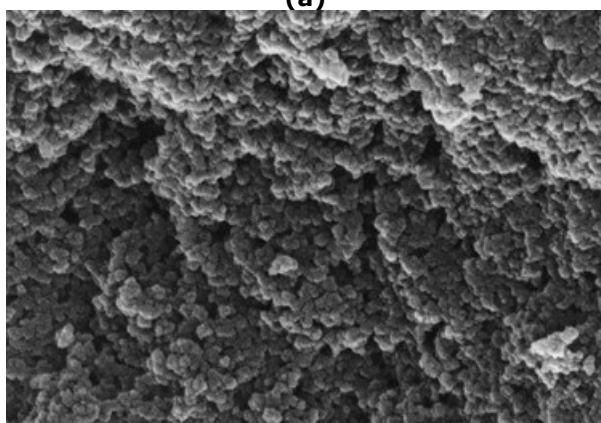
Figure 3(g) and (i) that the nanoparticles (Fe NPs or Zn NPs) formed between the carbon microspheres. The blown-up images of the nanoparticles in Figure 3(h) and (j) showed that Fe NPs were in spherical forms while Zn NPs were in lamellar forms.



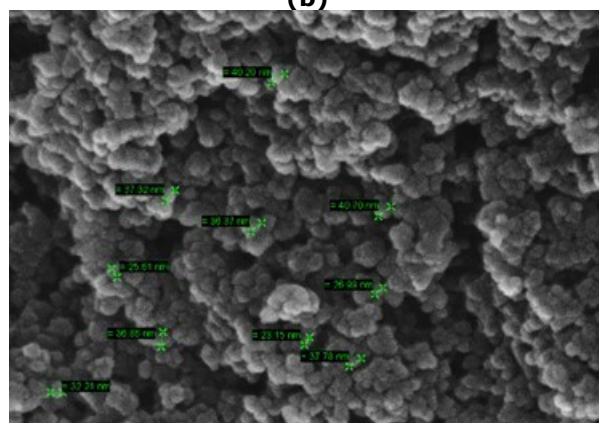
(a)



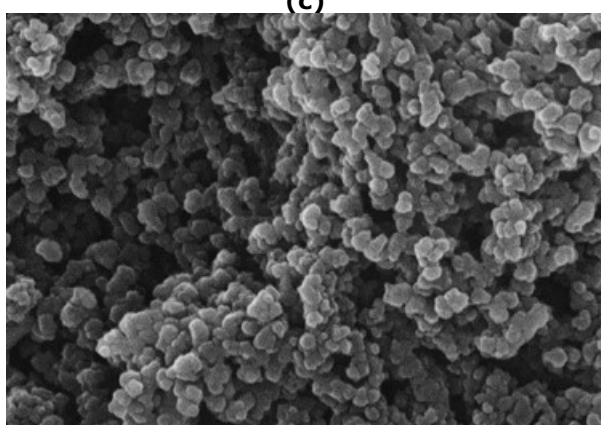
(b)



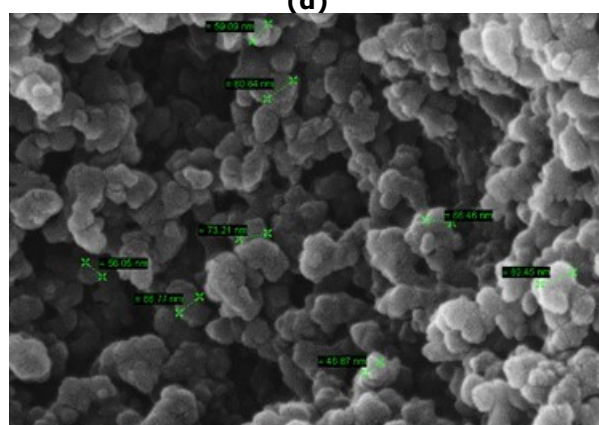
(c)



(d)



(e)



(f)

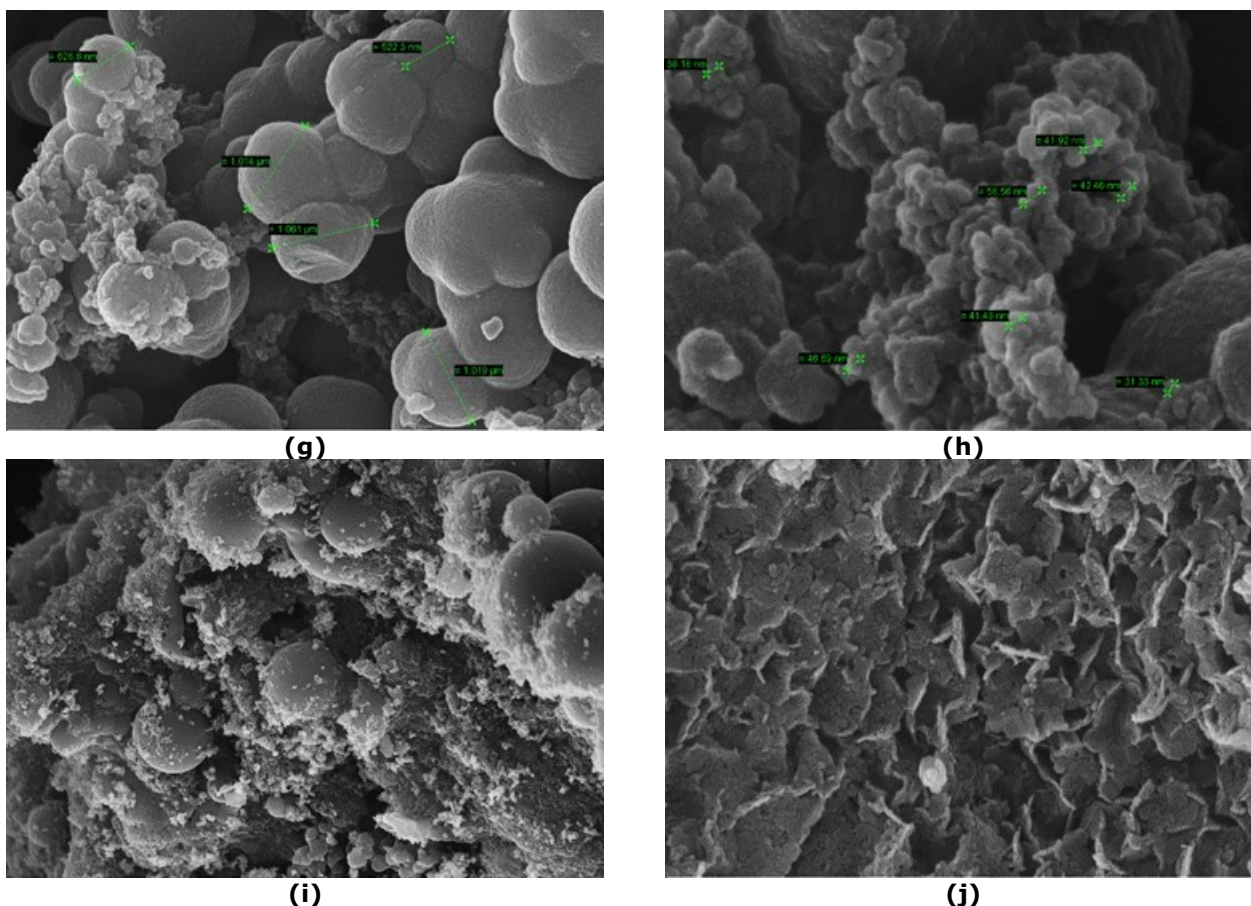


Figure 3. SEM images of **(a)** (Fe-Zn NPs)/C at 10.00 KX before the reaction, **(b)** (Fe-Zn NPs)/C at 30.00 KX before the reaction, **(c)** (Fe-Zn NPs)/C at 100.00 KX before the reaction, **(d)** (Fe-Zn NPs)/C at 200.00 KX before the reaction, **(e)** (Fe-Zn NPs)/C at 100.00 KX after the reaction, **(f)** (Fe-Zn NPs)/C at 200.00 KX after the reaction, **(g)** [(Fe NPs)/C] at 50.00 KX before the reaction, **(h)** [(Fe NPs)/C] at 200.00 KX before the reaction, **(i)** [(Zn NPs)/C] at 10.00 KX before the reaction, **(j)** [(Zn NPs)/C] at 100.00 KX before the reaction.

The specific surface area of (Fe-Zn NPs)/C was observed by using the following equation:

$$S = \frac{q \times N \times A}{M} \quad (\text{Eq. 1})$$

where S is the specific surface area (m^2/g (Fe-Zn NPs)/C), q is the maximum adsorption capacity of (Fe-Zn NPs)/C at the specific experimental conditions (g dye/g (Fe-Zn NPs)/C), N is the Avogadro's number (6.02×10^{23}); A is the cross-sectional area of methylene blue dye (m^2), and M is the molecular weight of methylene blue (18). In order to calculate the specific surface area, the methylene blue (MB) adsorption experiment with (Fe-Zn NPs)/C was carried out at 40°C , 100 mg/L initial dye concentration, natural pH (9.0), 1.0 g/L adsorbent concentration, and 480 min contact time. At these experimental conditions, the maximum adsorption capacity of (Fe-Zn NPs)/C for MB was determined to be 38.21 mg/g. The molecular weight and cross-sectional area of MB dye are 319 g/mole

and $1.2 \times 10^{-18} \text{ m}^2$ in a close-packed monolayer, respectively. By using these values, the specific surface area was calculated from Eq. (1) as 86.53 m^2/g (Fe-Zn NPs)/C.

A literature survey was performed for the comparison of specific surface area of nanoparticles-based hydrochar materials and the results were summarized in Table 1. Accordingly, except for the porous hydrochar materials, the specific surface area of (Fe-Zn NPs)/C synthesized in this study had relatively higher than the others. Therefore, it can be concluded that (Fe-Zn NPs)/C synthesized in this study could be evaluated as effective catalyst for the removal of NBB.

Table 1. Comparison of specific surface area of nanoparticles-based hydrochar materials

Material	Specific surface area (m ² /g)	Reference
Fe ₃ O ₄ -loaded coffee waste hydrochar	34.7	(19)
Fe-modified hydrochar from orange peel	72.5	(20)
Fe-Zn-oxide/hydrochar	76.8	(12)
(Fe-Zn NPs)/C	86.5	This work
Hydrochar functionalized Fe-Mn binary oxide nanocomposites	167.17	(21)
Zerovalent iron nanoparticles supported on hydrochar-derived porous carbon	423	(22)
Hydrochar-supported bimetallic Ni-Cu nanocatalysts	431.8	(23)
Iron nanoparticles immobilized into the porous hydrochar	446	(24)

Removal of NBB Dyestuff with Heterogeneous Fenton-like Reaction

Determination of Heterogeneous Fenton-like Catalyst Properties of (Fe-Zn NPs)/C and Its Compounds

The heterogeneous Fenton-like catalyst properties of (Fe-Zn NPs)/C and its compounds such as Fe-Zn NPs, Fe NPs/C, and Zn NPs/C were determined by calculating removal efficiencies of them for the selected model pollutant of NBB dyestuff removal. Accordingly, the color removal capacities of (Fe-Zn NPs)/C, [(FeNPs)/C], Fe-Zn NPs, and [(Zn NPs)/C] were 96.61, 68.08, 48.43, and 26.01 mg/g, respectively (experimental conditions: initial pH 3.0, 100 mg/L initial dyestuff concentration, 50 mM H₂O₂ concentration, 1.0 g/L catalyst concentration, 25 °C temperature). As a result, the Fenton-like removal studies for NBB dyestuff were performed with (Fe-Zn NPs)/C because it had the maximum color removal capacity among the other catalysts.

Effect of Environmental Conditions of Fenton-like Removal of NBB Dyestuff with (Fe-Zn NPs)/C

The initial pH of solution is a substantial parameter to design a treatment process. For this reason, the effect of initial pH on the removal of NBB dyestuff with (Fe-Zn NPs)/C was investigated at the experimental conditions of 100 mg/L initial dyestuff concentration, 50 mM H₂O₂ concentration, 1.0 g/L catalyst concentration, 25 °C temperature for the initial pH range of 3.0-5.0. The color removal capacities at the equilibrium time of 90 min in the initial pH range of 3.0-5.0 were shown in Figure 4. The color removal capacities at the equilibrium time of 90 min for initial pH 3.0, 5.0, 7.0, and 8.0 were determined to be 96.40±0.36, 95.59±0.61, 94.13±0.25, and 90.19±0.44 mg/g, respectively. Accordingly, the color removal capacities decreased slightly with the increase in the initial pH. Therefore, it could be suggested that this process enables studying at wide initial pH range, which is an advantage for industrial applications. The increase

of initial pH causes the decomposition of H₂O₂ to O₂ and H₂O; and so, fewer OH• radicals are formed during the reaction; as a result, the removal percentages reduce with the increase in the initial pH. Another reason may be the decrease in oxidation potentials of the produced OH• radicals at the higher initial pH values; and therefore, the removal percentages may be reduced with the increase in the initial pH (15). For these reasons, the studying at mild acidic conditions can be suggested for the removal of NBB dyestuff with (Fe-Zn NPs)/C.

The effect of H₂O₂ concentration on the removal of NBB dyestuff was investigated by varying H₂O₂ concentration from 1.0 mM to 50 mM at the other fixed conditions (initial pH, 3.0, initial dyestuff concentration, 100 mg/L, catalyst concentration, 1.0 g/L, temperature, 25 °C). The color removal capacities at the equilibrium time of 90 min in the H₂O₂ concentration range of 1.0-50 mM were shown in Figure 5. The color removal capacities at the equilibrium time of 90 min for H₂O₂ concentration of 1.0, 5.0, 10, 15, 25, and 50 mM were observed as 20.03±0.82, 55.51±0.41, 73.55±0.37, 85.57±0.42, 93.42±0.42, and 96.40±0.36 mg/g, respectively. As can be seen in Figure 5, the color removal capacities increased prominently with an increase in H₂O₂ concentration from 1.0 mM to 15 mM, and the increase rate thereafter declined. The reason for this slowdown in the increase rate at the higher H₂O₂ concentrations may be explained with the scavenging effect of OH• radical. At higher H₂O₂ concentrations, the formed OH• radicals reacted with H₂O₂ in the medium and the less oxidative radicals of HO₂• formed at the end of the reaction (H₂O₂ + OH• → HO₂• + H₂O), and so, the color removal amounts decreased at the higher H₂O₂ concentrations because there were fewer strong radicals of OH• in the medium (15). Consequently, because the maximum color removal capacity was obtained at 50 mM H₂O₂ concentration, the other experiments were carried out by using 50 mM H₂O₂.

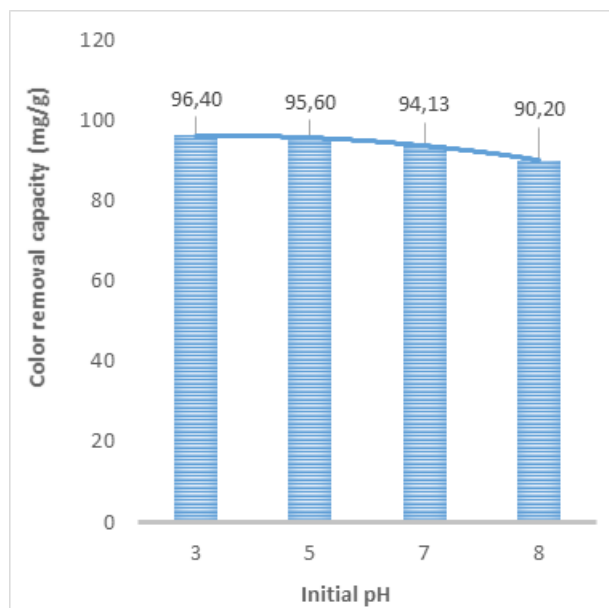


Figure 4. The effect of initial pH (experimental conditions: initial dyestuff concentration, 100 mg/L, H_2O_2 concentration, 50 mM, catalyst concentration, 1.0 g/L, temperature, 25°C)

The effect of temperature on the removal of NBB dyestuff with (Fe-Zn NPs)/C was investigated at the experimental conditions of initial pH of 3.0, initial dyestuff concentration, 100 mg/L, H_2O_2 concentration, 50 mM, catalyst concentration, 1.0 g/L for the temperature range of 25-55 °C. The color removal capacities in the temperature range of 25-55 °C were presented in Figure 6. The color removal capacities at the equilibrium time of 90 min for temperature of 25, 30, 40, 50, and 55 °C were

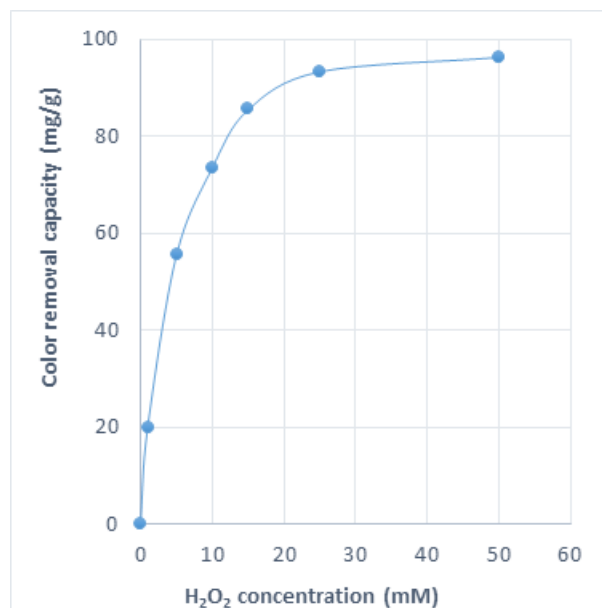


Figure 5. The effect of H_2O_2 concentration (experimental conditions: initial pH 3.0, 100 mg/L initial dyestuff concentration, 1.0 g/L catalyst concentration, 25°C temperature)

obtained to be 96.40 ± 0.36 , 98.68 ± 0.49 , 102.35 ± 0.23 , 97.98 ± 0.43 , and 85.55 ± 0.45 mg/g, respectively. As shown in Figure 6, the color removal capacity increased up to 40 °C, and then it decreased slightly. Accordingly, this process enables to study at the wide temperature range, which is an advantage for the industrial applications. On the other hand, the optimum temperature could be selected as 40 °C due to the obtained maximum color removal capacity at this temperature.

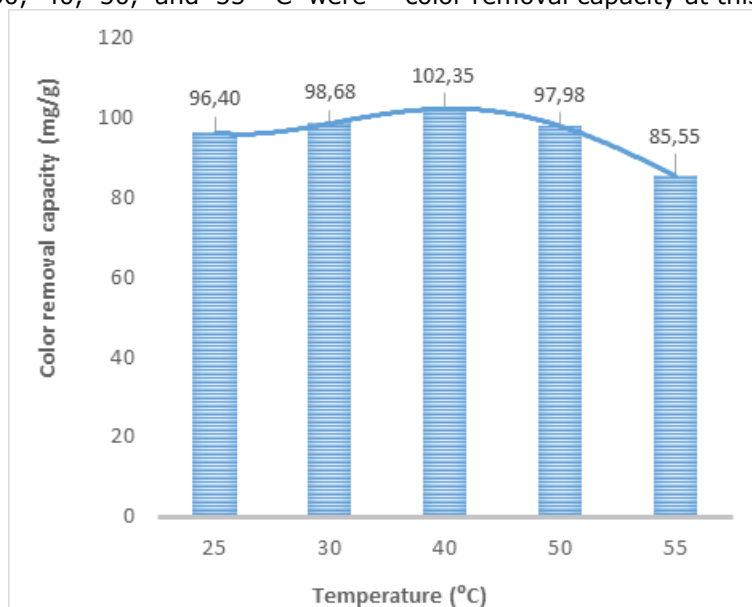


Figure 6. The effect of temperature (experimental conditions: initial pH, 3.0, initial dyestuff concentration, 100 mg/L, H_2O_2 concentration, 50 mM, catalyst concentration, 1.0 g/L).

The effect of initial dyestuff concentration on the removal of NBB dyestuff was investigated by varying initial dyestuff concentration from 100 mg/L to 1200

mg/L at the other fixed conditions (initial pH, 3.0, H_2O_2 concentration, 50 mM, catalyst concentration, 1.0 g/L, temperature, 40 °C). The color removal

capacities at the equilibrium time of 90 min in the initial dyestuff concentration range of 100-1200 mg/L were shown in Figure 7. The color removal capacities at the equilibrium time of 90 min for initial dye concentration of 100, 200, 300, 500, 700, 1000, and 1200 mg/L were determined as 102.35 ± 0.23 , 193.51 ± 0.41 , 266.53 ± 0.45 , 431.69 ± 0.35 , 524.59 ± 0.30 , 524.66 ± 0.46 , and 525.54 ± 0.41 mg/g, respectively. As can be seen in Figure 7, the color removal capacity increased up to 700 mg/L, and it remained nearly constant thereafter. This could be explained as follows (25):

(a) The increase in the initial dyestuff concentration causes adsorption of dyestuff molecules on the surface of catalyst, and so, dyestuff molecules adsorbed on the surface of catalyst may block the active sites of catalyst. As a result, fewer $\bullet\text{OH}$ radicals are formed and thus, the color removal capacities may decline.

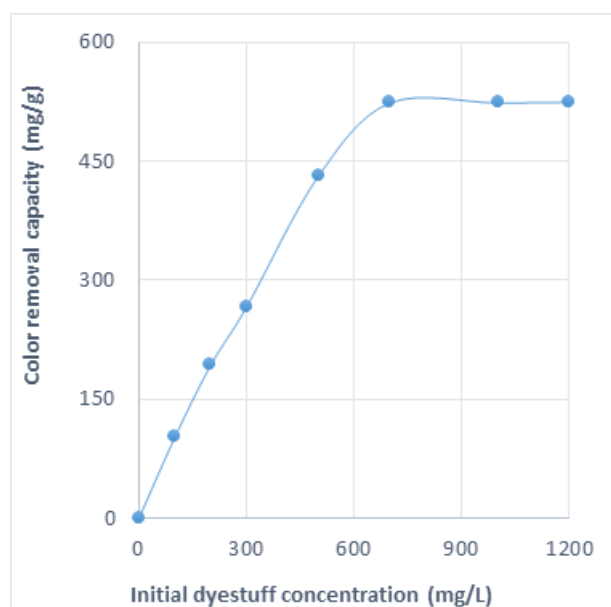


Figure 7. The effect of initial dyestuff concentration (experimental conditions: initial pH, 3.0, H_2O_2 concentration, 50 mM, catalyst concentration, 1.0 g/L, 40 °C temperature)

The effect of catalyst concentration on the removal of NBB dyestuff with (Fe-Zn NPs)/C was investigated at the experimental conditions (initial pH, 3.0, initial dyestuff concentration, 100 mg/L, H_2O_2 concentration, 50 mM, temperature, 40 °C for the catalyst concentration range of 0.25-3.0. The color removal capacities at the equilibrium time of 90 min in the catalyst concentration range of 0.25-3.0 were shown in Figure 9. The color removal capacities at the equilibrium time of 90 min for catalyst concentration of 0.25, 0.50, 1.0, 2.0, and 3.0 g/L were obtained as 472.84 ± 0.42 , 216.98 ± 0.39 , 102.35 ± 0.23 , 75.71 ± 0.51 , and 72.39 ± 0.49 mg/g, respectively. As seen in the figure, color removal capacities decreased with increasing catalyst

(b) When there are more dyestuff molecules in the reaction medium, they compete against the intermediates produced during the Fenton-like reaction and thus, the color removal capacities may decline.

The effect of contact time on the removal of NBB dyestuff was investigated by varying initial dyestuff concentration from 100 mg/L to 1200 mg/L at the other fixed conditions (initial pH, 3.0, H_2O_2 concentration, 50 mM, catalyst concentration, 1.0 g/L, temperature, 40 °C). The changes of color removal capacities with contact time for the different initial dyestuff concentrations were shown in Figure 8. As can be seen in Figure 8, the removal capacities increased by increasing contact time up to 90 min and then remained constant indicating that a maximum removal was attained. Therefore, the equilibrium time for the removal of NBB dyestuff with (Fe-Zn NPs)/C was determined to be 90 min.

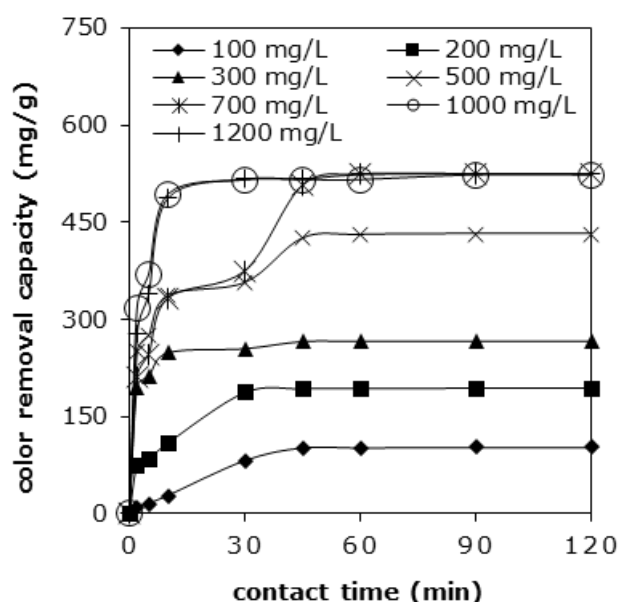


Figure 8. The effect of contact time (experimental conditions: initial pH, 3.0, H_2O_2 concentration, 50 mM, catalyst concentration, 1.0 g/L, 40 °C temperature)

concentration. In general, color removal capacity is expected to increase with the increase in the catalyst concentration because the more catalysts are present in the reaction medium, the more H_2O_2 is expected to decompose to $\text{OH}\bullet$ radicals. However, it has been reported in the literature that the excessive catalyst loading causes a decrease in the color removal due to the scavenging effect of $\text{OH}\bullet$ radicals. Accordingly, the formed $\text{OH}\bullet$ radicals react with the excess iron ions in the reaction medium, arising from the iron based catalyst, ($\text{Fe}^{2+} + \text{OH}\bullet \rightarrow \text{Fe}^{3+} + \text{OH}^-$) (26). For the same reason, the catalyst concentrations higher than 0.25 g/L caused the reduction of the color removal capacities in this study, the optimum catalyst concentration was

therefore determined as 0.25 g/L.

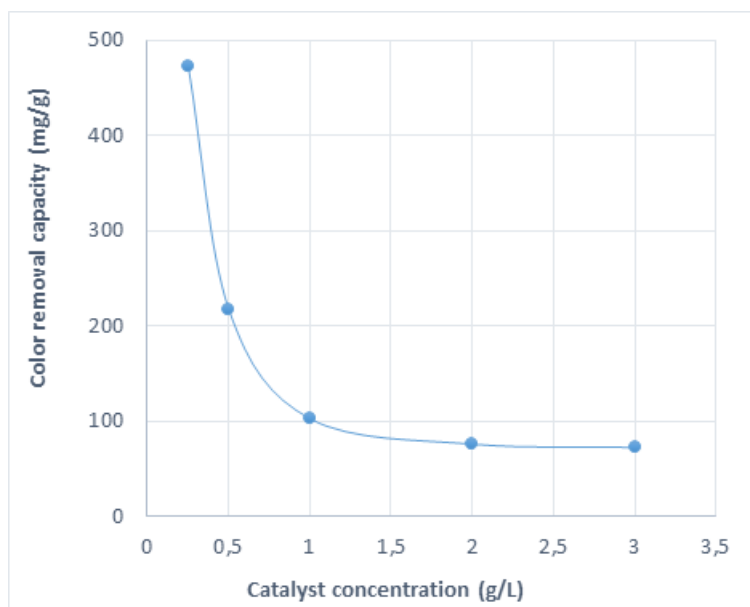


Figure 9. Effect of catalyst concentration (experimental conditions: initial pH, 3.0, initial dyestuff concentration, 100 mg/L, H₂O₂ concentration, 50 mM, temperature, 40°C).

The optimum experimental conditions of this Fenton-like reaction were determined as follows: initial pH, 3.0, H₂O₂ concentration, 50 mM, temperature, 40 °C, and catalyst concentration, 0.25 g/L. At these conditions for initial dye concentration of 100 mg/L, color removal and COD removal percentages were obtained as 100% and 37.6±3.75%, respectively. Although the color removal percentage of 100% showed that the chromophore group of NBB was completely destroyed, the COD removal percentage of 37.6±3.75% indicated the partially oxidation of the dye molecules to CO₂ and H₂O.

A literature survey was performed for the comparison of color removal methods for NBB removal and the results were summarized in Table 2. Accordingly, NBB removal with heterogeneous Fenton-like reaction was firstly evaluated in the literature with this study and in this study, the color removal that could be competitive with other removal methods has been achieved at mild conditions. Moreover, it is an important advantage of this study that 100% color removal can be achieved at the higher initial dye than the most of the studies given in Table 2, which could provide treating the wastewaters containing high dye concentrations.

Table 2. Comparison of color removal methods for NBB removal.

Method of color removal	Experimental conditions	Percentage of color removal (%)	Reference
Fenton-like reaction	Initial dye concentration: 100 mg/L , pH: 3.0, H ₂ O ₂ concentration: 50 mM, temperature: 40 °C, catalyst concentration: 0.25 g/L	100	This work
Microwave assisted adsorption	Microwave power: 20 W, pH: 3, initial dye concentration: 2.5 mg/L , catalyst amount: 50 mg	100	(27)
Sonolytic degradation	Initial dye concentration: 5 mg/L , persulfate concentration: 500 mg/L, frequency: 1700 kHz, temperature: 25 °C, pH: 6.0	100	(28)
Sonolytic degradation	Initial dye concentration: 5 mg/L , temperature: 25 °C, natural pH, frequency: 585 kHz	100	(29)
Photo-catalytic degradation	PH: 3, initial dye concentration: 15 mg/L , catalyst concentration: 1 g/L	99.74	(30)
Sono-photo-catalytic degradation	Initial pH: 11.0, H ₂ O ₂ concentration: 44.1 mmol/L, Fe-TiO ₂ catalyst concentration: 2.2 g/L	96	(31)

Persulfate (PS) assisted sonochemical degradation	Initial dye concentration: 5 mg/L , initial PS concentration: 9 mg/L, temperature: 25 °C, pH: 6, frequency: 585 kHz	95	(32)
Removal using enzyme (HRP)	Initial dye concentration: 370 mg/L , H ₂ O ₂ concentration: 0.3 mmol/L, enzyme concentration: 5.88 U/mL, temperature: 70 °C	94.7	(33)
Photo-catalytic degradation	Initial dye concentration: 20 mg/L , catalyst concentration: 1 g/L, 500 W xenon lamp	94.3	(34)
Sonochemical removal	Initial dye concentration: 5 mg/L , temperature: 25 °C, pH=6, frequency: 585 kHz	94	(35)
Photo-catalytic degradation	Initial dye concentration: 10 mg/L , P25@Pd/C catalyst concentration: 0.1 g/L, time: 120 min, 150 W Tungsten lamp, temperature: 25 °C	91	(36)
Solar photo-catalytic degradation	Initial dye concentration: 123 mg/L , AgBr-ZnO catalyst concentration: 2 g/L, pH=11, flow rate of air: 8.1 mL/s	50.8	(37)

Reaction Kinetics

In order to elucidate the kinetics of degradation of NBB with (Fe-Zn NPs)/C, kinetic data were obtained under optimum conditions (initial pH: 3.0, temperature: 40 °C, catalyst concentration: 0.25 g/L) and then, the reaction rate expression was determined by performing mathematical analysis with the initial rate method.

Firstly, a reaction rate expression was suggested as shown in the following equation (Eq. 2):

$$-dC/(X_0 \cdot dt) = -dC^*/dt = k \cdot C^n \quad (\text{Eq. 2})$$

where C is the remaining dye concentration (mg/L), X_0 is the catalyst concentration (g/L), t is the reaction time (min), $-dC^*/dt$ is the degradation reaction rate for unit mass of catalyst (mg/(g_{cat}·min)), k is the degradation reaction rate constant, n is the order of degradation.

The linear form of Equation (2) according to the initial rate method was presented in Equation (3):

$$\ln(-dC^*/dt) = \ln k + n \cdot \ln(C_0) \quad (\text{Eq. 3})$$

In order to calculate the values of $(-dC^*/dt)$, the remaining dye concentrations ($C^*=C_t/X_0$) against the reaction time was plotted for the different initial dye concentrations (C_0). Then, the tangent lines were drawn at $t=0$ to the curves obtained for the different initial dye concentrations and the slopes of these tangent lines gave the values of $(-dC^*/dt)$.

After that, $\ln(-dC^*/dt)$ vs $\ln(C_0)$ was plotted (given in Figure 10) and then, from the slope and intercept of the obtained linear line, the order of degradation (n) and the rate constant of the degradation (k) were calculated, respectively (38).

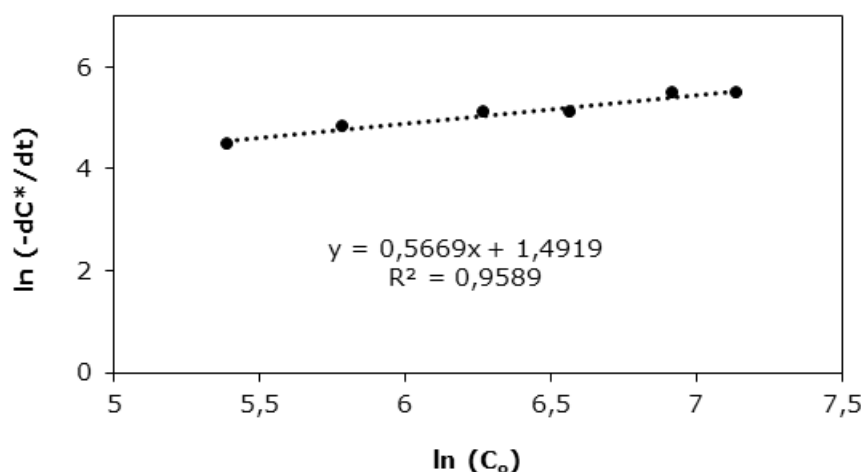


Figure 10. The plot of $(-dC^*/dt)$ vs $\ln(C_0)$ (initial pH: 3.0, temperature: 40 °C, catalyst concentration: 0.25 g/L).

The order of degradation (n) and rate constant of the degradation (k) were calculated as 0.5669 and 4.45, respectively. Accordingly, the reaction rate expression could be written as $-r_{\text{degradation}} (\text{mg}/(\text{g}_{\text{cat}} \cdot \text{min})) = 4.45(C)^{0.5669}$.

CONCLUSION

In this study, iron-zinc nanoparticles (Fe-Zn NPs) were firstly synthesized in the presence of glucose

by co-precipitation method using NaOH and then, the iron-zinc nanoparticles/carbon composite (Fe-Zn NPs)/C was synthesized by the hydrothermal carbonization of glucose in the solution containing Fe-Zn NPs. Next, the usability of [(Fe-ZnNPs)/C] as a heterogeneous catalyst in the removal of NBB dyestuff via Fenton-like reaction was investigated. Using the hydrochar as a supporter material for the nanoparticles provide not only lower the cost of the catalyst but also increase the catalytic activity by improving the catalyst properties. The removal could be achieved when both oxidant (H_2O_2) and catalyst (Fe-Zn NPs)/C were present together in the reaction medium, thus proving that the dyestuff was decolorized by Fenton-like reaction. The studies showed that the optimum initial pH, H_2O_2 concentration, temperature, and catalyst concentration for Fenton-like removal of NBB dyestuff with

[(Fe-ZnNPs)/C] were determined to be 3.0, 50 mM, and 0.25 g/L, respectively. The Fenton-like reaction order and rate constant were calculated as 0.5669 and 4.45, respectively. Moreover, this process enables to study at the wide initial pH and temperature range, which is an important advantage for the industrial applications. Consequently, the present study has revealed significant outputs to the synthesis of an effective Fenton-like heterogeneous catalyst, which could be important for the contribution to the related literature as well as the water treatment applications.

ACKNOWLEDGMENTS

This study was presented in 2nd Cilicia International Symposium on Engineering and Technology (CISSET 2019) as an oral presentation and evaluated by Journal of the Turkish Chemical Society Section B: Chemical Engineering.

REFERENCES

- Kumar V, Ghime D, Ghosh P. Decolorization of textile dye Rifafix Red 3BN by natural hematite and a comparative study on different types of Fenton process. *Chem Eng Commun* [Internet]. 2019;0(0):1-10. Available from: <https://doi.org/10.1080/00986445.2019.1652603>
- Tarkwa JB, Oturan N, Acayanka E, Laminsi S, Oturan MA. Photo-Fenton oxidation of Orange G azo dye: process optimization and mineralization mechanism. *Environ Chem Lett* [Internet]. 2019;17(1):473-9. Available from: <https://doi.org/10.1007/s10311-018-0773-0>
- Katheresan V, Kansedo J, Lau SY. Efficiency of various recent wastewater dye removal methods: A review. *J Environ Chem Eng*. 2018;6(4):4676-97.
- Khan J, Tariq M, Muhammad M, Mehmood MH, Ullah I, Raziq A, Akbar F, Saqib M, Rahim A, Niaz A. Kinetic and thermodynamic study of oxidative degradation of acid yellow 17 dye by fenton-like process: effect of HCO_3^- , CO_3^{2-} , Cl^- and SO_4^{2-} on dye degradation. *Bull. Chem. Soc. Ethiop*. 2019;33(2):243-54.
- Gu T, Dong H, Lu T, Han L, Zhan Y. Fluoride ion accelerating degradation of organic pollutants by Cu(II)-catalyzed Fenton-like reaction at wide pH range. *J Hazard Mater* [Internet]. 2019;377(January):365-70. Available from: <https://doi.org/10.1016/j.jhazmat.2019.05.073>
- Vu AT, Xuan TN, Lee CH. Preparation of mesoporous $\text{Fe}_2\text{O}_3\cdot\text{SiO}_2$ composite from rice husk as an efficient heterogeneous Fenton-like catalyst for degradation of organic dyes. *J Water Process Eng* [Internet]. 2019;28(January):169-80. Available from: <https://doi.org/10.1016/j.jwpe.2019.01.019>
- Yavari S, Mahmodi NM, Teymouri P, Shahmoradi B, Maleki A. Cobalt ferrite nanoparticles: Preparation, characterization and anionic dye removal capability. *J Taiwan Inst Chem Eng* [Internet]. 2016;59:320-9. Available from: <http://dx.doi.org/10.1016/j.jtice.2015.08.011>
- Ma Q, Cui L, Zhou S, Li Y, Shi W, Ai S. Iron nanoparticles in situ encapsulated in lignin-derived hydrochar as an effective catalyst for phenol removal. *Environ Sci Pollut Res*. 2018;25(21):20833-40.
- Gai C, Zhu N, Hoekman SK, Liu Z, Jiao W, Peng N. Highly dispersed nickel nanoparticles supported on hydrochar for hydrogen-rich syngas production from catalytic reforming of biomass. *Energy Convers Manag* [Internet]. 2019;183(January):474-84. Available from: <https://doi.org/10.1016/j.enconman.2018.12.121>
- Wang T, Zhai Y, Zhu Y, Li C, Zeng G. A review of the hydrothermal carbonization of biomass waste for hydrochar formation: Process conditions, fundamentals, and physicochemical properties. *Renew Sustain Energy Rev* [Internet]. 2018;90(December 2016):223-47. Available from: <https://doi.org/10.1016/j.rser.2018.03.071>
- Basso D, Castello D, Baratieri M, Fiori L. Hydrothermal carbonization of waste biomass: progress report and prospects. 21st Eur Biomass Conf Exhib. 2013;(June):1478-87.
- Liang C, Liu Y, Li K, Wen J, Xing S, Ma Z. Heterogeneous photo-Fenton degradation of organic pollutants with amorphous Fe-Zn-oxide/hydrochar under visible light irradiation. *Sep Purif Technol* [Internet]. 2017;188:105-11. Available from: <http://dx.doi.org/10.1016/j.seppur.2017.07.027>

13. Kang SM, Li XL, Fan J, Chang J, Characterization of Hydrochars Produced by Hydrothermal Carbonization of Lignin, Cellulose, D-Xylose, and Wood Meal. *Ind Eng Chem Res* [Internet]. 2012;51:9023–9031. Available from: <http://dx.doi.org/10.1021/ie300565d>
14. Chen XY, Chen C, Zhang ZJ, Xie DH, Liu JW, Nitrogen/manganese oxides doped porous carbons derived from sodium butyl naphthalene sulfonate. *J Colloid Interf Sci* [Internet]. 2013;398:176–184. Available from: <http://dx.doi.org/10.1016/j.jcis.2013.01.068>
15. Khataee A, Kayan B, Kalderis D, Karimi A, Akay S, Konsolakis M. Ultrasound-assisted removal of Acid Red 17 using nanosized Fe₃O₄-loaded coffee waste hydrochar. *Ultrason Sonochem* [Internet]. 2017;35:72–80. Available from: <http://dx.doi.org/10.1016/j.ultsonch.2016.09.004>
16. Liu Z, Zhang F, Hoekman SK, Liu T, Gai C, Peng N. Homogeneously Dispersed Zerovalent Iron Nanoparticles Supported on Hydrochar-Derived Porous Carbon: Simple, in Situ Synthesis and Use for Dechlorination of PCBs. *ACS Sustain Chem Eng*. 2016;4(6):3261–7.
17. Gai C, Zhang F, Lang Q, Liu T, Peng N, Liu Z. Facile one-pot synthesis of iron nanoparticles immobilized into the porous hydrochar for catalytic decomposition of phenol. *Appl Catal B Environ* [Internet]. 2017;204:566–76. Available from: <http://dx.doi.org/10.1016/j.apcatb.2016.12.005>
18. Uzunoğlu D, Gürel N, Özkaya N, Özer A. The single batch biosorption of copper (II) ions on *Sargassum acinarum*. *Desalin Water Treat* [Internet]. 2014;52(7-9), 1514-1523. Available from: <https://doi.org/10.1080/19443994.2013.789403>
19. Khataee A, Kayan B, Kalderis D, Karimi A, Akay S, Konsolakis M. Ultrasound-assisted removal of Acid Red 17 using nanosized Fe₃O₄-loaded coffee waste hydrochar. *Ultrason Sonochem* [Internet]. 2017;35, 72-80. Available from: <https://doi.org/10.1016/j.ultsonch.2016.09.004>
20. Çatlıoğlu FN, Akay S, Gözmen B, Turunc E, Anastopoulos I, Kayan B, Kalderis D. Fe-modified hydrochar from orange peel as adsorbent of food colorant Brilliant Black: process optimization and kinetic studies. *Int J Environ Sci Tec* [Internet]. 2020;17:1975–1990. Available from: <https://doi.org/10.1007/s13762-019-02593-z>
21. Ning Q, Liu Y, Liu S, Jiang L, Zeng G, Zeng Z, Kare Z. Fabrication of hydrochar functionalized Fe–Mn binary oxide nanocomposites: characterization and 17 β -estradiol removal. *Rsc Advances* [Internet]. 2017;7(59), 37122-37129. Available from: <https://doi.org/10.1039/c7ra06065c>
22. Liu Z, Zhang F, Hoekman SK, Liu T, Gai C, Peng N. Homogeneously dispersed zerovalent iron nanoparticles supported on hydrochar-derived porous carbon: simple, in situ synthesis and use for dechlorination of PCBs. *ACS Sustain Chem Eng* [Internet]. 2016;4(6), 3261-3267. Available from: <https://doi.org/10.1021/acssuschemeng.6b00306>
23. Gai C, Yang T, Liu H, Liu Z, Jiao W. Hydrochar-Supported Bimetallic Ni–Cu Nanocatalysts for Sustainable H₂ Production. *ACS Appl. Nano Mater* [Internet]. 2019;2(11), 7279-7289. Available from: <https://doi.org/10.1021/acsanm.9b01762>
24. Gai C, Zhang F, Lang Q, Liu T, Peng N, Liu Z. Facile one-pot synthesis of iron nanoparticles immobilized into the porous hydrochar for catalytic decomposition of phenol. *Appl Catal B* [Internet]. 2017;204, 566-576. Available from: <http://dx.doi.org/10.1016/j.apcatb.2016.12.005>
25. Hassani A, Çelikdağ G, Eghbali P, Sevim M, Karaca S, Metin Ö. Heterogeneous sono-Fenton-like process using magnetic cobalt ferrite-reduced graphene oxide (CoFe₂O₄-rGO) nanocomposite for the removal of organic dyes from aqueous solution. *Ultrason Sonochem*. 2018;40(August 2017):841–52.
26. Wang N, Zheng T, Zhang G, Wang P. A review on Fenton-like processes for organic wastewater treatment. *J Environ Chem Eng* [Internet]. 2016;4(1):762–87. Available from: <http://dx.doi.org/10.1016/j.jece.2015.12.016>
27. Ahmed SA, Soliman EM. Silica coated magnetic particles using microwave synthesis for removal of dyes from natural water samples: Synthesis, characterization, equilibrium, isotherm and kinetics studies. *Appl Surf Sci* [Internet]. 2013;284:23–32. Available from: <http://dx.doi.org/10.1016/j.apsusc.2013.06.129>
28. Ferkous H, Merouani S, Hamdaoui O. Sonolytic degradation of naphthol blue black at 1700kHz: Effects of salts, complex matrices and persulfate. *J Water Process Eng* [Internet]. 2016;9:67–77. Available from: <http://dx.doi.org/10.1016/j.jwpe.2015.11.003>
29. Ferkous H, Merouani S, Hamdaoui O, Rezgui Y, Guemini M. Comprehensive experimental and numerical investigations of the effect of frequency and acoustic intensity on the sonolytic degradation of naphthol blue black in water. *Ultrason Sonochem* [Internet]. 2015;26:30–9. Available from: <http://dx.doi.org/10.1016/j.ultsonch.2015.02.004>

30. Debnath S, Ballav N, Nyoni H, Maity A, Pillay K. Optimization and mechanism elucidation of the catalytic photo-degradation of the dyes Eosin Yellow (EY) and Naphthol blue black (NBB) by a polyaniline-coated titanium dioxide nanocomposite. *Appl Catal B Environ* [Internet]. 2015;163:330–42. Available from: <http://dx.doi.org/10.1016/j.apcatb.2014.08.011>
31. Reddy DR, Dinesh GK, Anandan S, Sivasankar T. Sonophotocatalytic treatment of Naphthol Blue Black dye and real textile wastewater using synthesized Fe doped TiO₂. *Chem Eng Process Process Intensif*. 2016;99:10–8.
32. Ferkous H, Merouani S, Hamdaoui O, Pétrier C. Persulfate-enhanced sonochemical degradation of naphthol blue black in water: Evidence of sulfate radical formation. *Ultrason Sonochem* [Internet]. 2017;34:580–7. Available from: <http://dx.doi.org/10.1016/j.ultsonch.2016.06.027>
33. Onder S, Celebi M, Altikatoglu M, Hatipoglu A, Kuzu H. Decolorization of naphthol blue black using the horseradish peroxidase. *Appl Biochem Biotechnol*. 2011;163(3):433–43.
34. Mamba G, Mbianda XY, Mishra AK. Photocatalytic degradation of the diazo dye naphthol blue black in water using MWCNT/Gd,N,S-TiO₂ nanocomposites under simulated solar light. *Environ Sci (China)* [Internet]. 2015;33:219–28. Available from: <http://dx.doi.org/10.1016/j.jes.2014.06.052>
35. Ferkous H, Hamdaoui O, Merouani S. Sonochemical degradation of naphthol blue black in water: Effect of operating parameters. *Ultrason Sonochem* [Internet]. 2015;26:40–7. Available from: <http://dx.doi.org/10.1016/j.ultsonch.2015.03.013>
36. Krishnakumar B, Kumar S, Gil JM, Pandiyan V, Aguiar A, Sobral AJFN. Highly active P25@Pd/C nanocomposite for the degradation of Naphthol Blue Black with visible light. *J Mol Struct*. 2018;1153:346–52.
37. Krishnakumar B, Swaminathan M. Solar photocatalytic degradation of Naphthol Blue Black. *Desalin Water Treat*. 2013;51(34–36):6572–9.
38. Fogler, H. Scott. *Elements Of Chemical Reaction Engineering*. Upper Saddle River, N.J. Prentice Hall International Editions, 3rd Edition, Page: 231.

